Research on Engineering Structures & Materials
journal homepage: http://www.jresm.org
Research Group

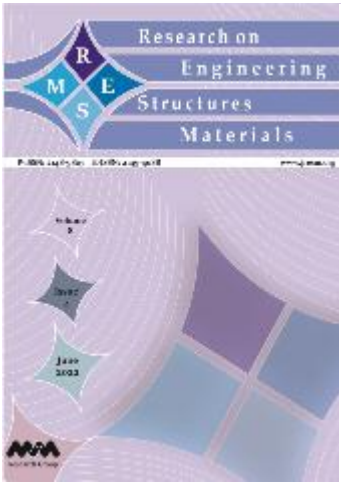

Weldability of interlocked-end friction stir welding of aluminum alloy: single and double-sided welding

Olatunji Oladimeji Ojo, Gbadebo Samuel John

Online Publication Date: 10 Aug 2022

URL: http://www.jresm.org/archive/resm2022.439me3005.html
DOI: http://dx.doi.org/10.17515/resm2022.439me3005

Journal Abbreviation: *Res. Eng. Struct. Mater.*

To cite this article
Ojo OO, John GS. Weldability of interlocked-end friction stir welding of aluminum alloy: single and double-sided welding. *Res. Eng. Struct. Mater.*, 2022; 8(4): 735-749.

Research on Engineering Structures & Materials
journal homepage: http://www.jresm.org
Research Group

Research Article

Weldability of interlocked-end friction stir welding of aluminum alloy: single and double-sided welding

Olatunji Oladimeji Ojo*[1,3,a], Gbadebo Samuel John[2,3,b]

[1]*Department of Industrial and Production Engineering, Federal University of Technology Akure, Nigeria.*
[2]*Department of Mechanical Engineering, Ogun State Institute of Technology Igbesa, Nigeria.*
[3]*Department of Mechanical Engineering, Federal University of Technology Akure, Nigeria.*

Article Info

Article history:

Received 30 May 2022
Revised 05 Aug 2022
Accepted 07 Aug 2022

Keywords:

Weldability;
Interlocked end friction stir welding;
Aluminum alloy;
Weld structure;
Tensile strength;
Fracture

Abstract

The weldability of the interlocked-end friction stir welding (IFSW) of aluminum plates was studied via the use of single and double-sided welding procedures. The abutting ends of the Al plates were milled into equidistant slots (with 5 mm rise and 10 mm span) and an interlocked/meshed end profile was formed when two slotted plates were brought together. The friction stir welding of the interlocked end of the plates was carried out at different tool rotational (700 – 1120 rpm) and traverse (21 – 63 mm/min) speeds while the structure, tensile strength, and fracture behaviors of the resultant welds were examined. The results showed the presence of flow-induced defects in the welds irrespective of the adopted welding procedure. Relative to the single-sided welds, the severity of the weld defect was significantly reduced in the double-sided welds due to dual material plasticization, material consolidation, and twofold recrystallization advantages. Improved tensile strength (from 39.6 to 69.1 MPa), reduced area fraction of flow-induced defect, and a large area with ductile features are obtained in the double-sided IFSW weld. A double-sided welding procedure is recommended for the interlocked-end friction stir welding process.

1. Introduction

Aluminum alloys are used in automotive, aerospace, marine applications, and high-speed train manufacturing because of their high strength, corrosion resistance, and high ductility [1]. Welding of Al alloy with fusion and other means always introduces challenges like distortion, porosity and blowholes, hot cracking, and excess heat to aluminum welds [2]. Solid-state friction stir welding (FSW) of Al alloy can effectively remove these challenges as the FSW process takes place at a temperature below the melting point of Al alloys [3][4]. Tool design modifications [5][6], process parameter optimization [7-10], and variance of the FSW/FSSW process [11-15] have been successfully utilized in improving the mechanical properties of friction stir welds of Al alloys in literature. Meanwhile, modification of joint-line/configuration is adjudged as a worthy alternative/route for improving the performance of dissimilar and similar friction stir welds, which is yet to receive concerted efforts in literature. Limited studies have been carried out on the alteration of joint-line/configuration for the improvement of weld strength [5][16][17]. Thus, this paper attempts to modify/change the abutting line of the conventional friction stir welding process to an interlocked end and studies the weld strength and fracture behavior of the resultant joints under varied process parameters.

Some of the existing works in the literature on the modifications of joint-line/configuration have shown good prospects while improvements are still pertinent via continuous studies.

*Corresponding author: ojooladimeji90@yahoo.com
[a] orcid.org/0000-0002-6581-1168; [b] orcid.org/0000-0001-6693-0188
DOI: http://dx.doi.org/10.17515/resm2022.439me3005

For instance, cuboid-shaped grooves were machined at the abutting ends of the Ti–6Al–4V and aluminum alloys before the lap-butt friction stir welding of the alloys in the studies of Li et al. [18]. It was reported that up to 92 % of the Al alloy's tensile strength was achieved as the tensile fracture resistance of the joint. Kumar et al. [11] also utilized the same lap-butt joint configuration (cuboid-shaped grooves) to join AA6061-T6 and AZ31B magnesium alloys, and a joint efficiency of 61% was obtained. Acharya et al [19] investigated the double-butt-lap (DBL) joint configuration of the AA6061-T6 Al alloy and the obtained result was compared with that of the single-square-butt (SSB) joints. The DBL joints showed better tensile strength as compared to the SSB joints. Pankul et al. [5] investigated the friction stir welding of the AA6063 aluminum alloy by changing the conventional butt geometry to an inclined butt (scarf configuration). This welding approach was reported to be susceptible to undesirable flow defects such as tunnel, hooking, kissing, and zigzag line due to the inherent low inclined angle of 26° to the vertical. In addition, the scarf configuration-produced joint was acknowledged to have low loadbearing resistance in comparison to the butt/conventional friction stir welded counterparts. In the search for better strength in scarf configuration, Sethi et al. [20] increased the angle of inclination to 60° using AA6061-T6 Al alloy as the base material. The increase in the angle of inclination improved the tensile strength of the joint by 13.5% over the sample produced by the square butt configuration. Similarly, Reza-E-Rabby et al. [16] also investigated the dovetail (head-tail) FSW of the rolled homogeneous armor steel (as the head) and AA6061 Al (as the tail) alloys. An improvement in tensile strength (4000 N/mm) was obtained via this welding approach.

Recently, Zhang et al [21] conducted tooth-shaped joint configuration-based friction stir welding on dissimilar copper and aluminum alloy. The tooth was designed to have equal width and height of 3 mm. It was reported that the disparity in the properties of the base materials negatively affected the flowability and the resultant metallurgical bonding of the joint. The impact of tooth-shaped joint configuration on the properties of similar alloys is yet to be explicated in the literature. This study utilizes a somewhat similar joining approach, otherwise referred to as the interlock-end friction stir welding process to join Al alloy sheets having equal thicknesses to unravel the gap in literature. Rises and spans were machined along the abutting ends of the Al plates in such a manner that when the plates were brought together, they formed an interlocked end. The rise of the interlocked end was designed to be higher than the span to form a symmetric profile after the machined ends of the sheets were brought together in this study. The AA1050 aluminum alloy has industrial applications in the fabrication of chemical process plant equipment, architectural flashings, lamb reflectors, and food containers due to its high corrosion resistance [22]. Thus, the AA1050 Al alloy was employed as the base material for this study. This paper investigated the weldability of the interlock-end friction stir welding (IFSW) of AA1050 Al alloy while areas such as the structure, tensile strength, and fracture behaviors of the IFSW joints were covered.

2. Materials and Method

Commercial rolled AA1050 aluminum alloy plates having a thickness of 6 mm were utilized as the base metal. Table 1 reveals the chemical composition of the base metal. The as-received Al plates were cleaned with acetone to remove the inherent dirt and were subsequently cut into the dimensions of 100 x 50 mm x 6 mm on a guillotine machine. Before the interlocked-end friction stir welding (IFSW) process, the preliminary edge preparation (or cutting of the rise and span) was performed on the abutting ends of the Al plates on a milling machine. Fig. 1 shows the equidistant slots (having a rise of 5 mm and a span of 10 mm) that were milled out along the 100 mm length of the cut Al samples.

Table 1. Chemical Composition of base metal (Wt %)

Element	Mg	Si	Mn	Ni	Zn	Fe	Ti	Ga	Al
Wt%	0.011	0.065	0.003	0.004	0.003	0.336	0.026	0.018	Bal.

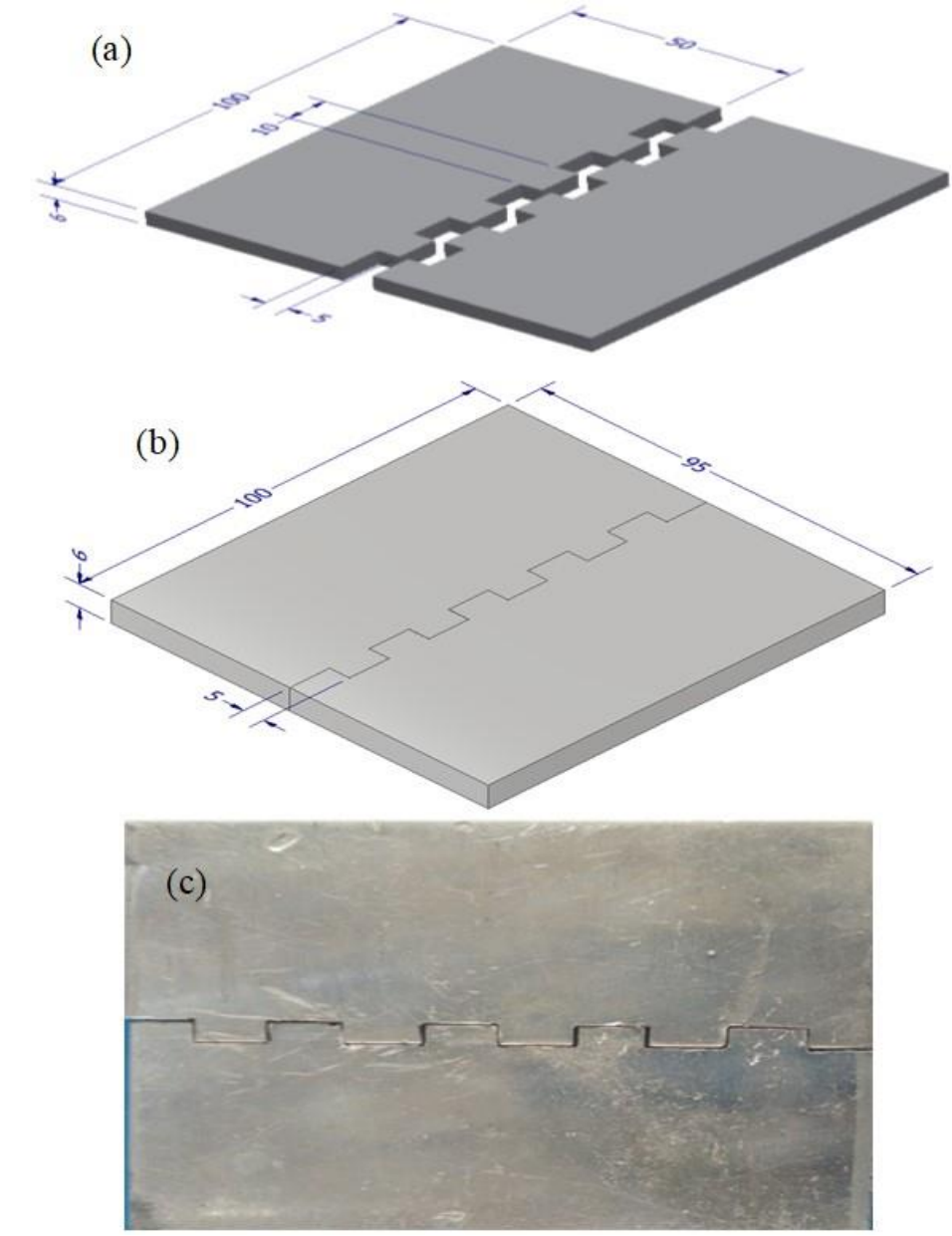

Fig. 1 Interlock-end configuration for the welding process: (a) schematic of the milled ends showing rises and spans, (b) schematic of the meshed/interlocked ends (c) actual meshed/interlocked-ends

The interlocked-end friction stir welding (IFSW) process was then carried out along the interlocked/meshed end of the plates. A 20 mm diameter HSS tool steel was selected for

the welding process. Pin and pinless tools were fabricated from the HSS tool for the welding process. Meanwhile, the design of the pin tool was based on the joint configurations. Since the rise in the interlock-end was 5 mm (see Fig.1), the pin diameter of 7 mm was fabricated to accommodate the interlocked zone and ensure proper intermixing when the pin is plunged into the setup of the workpiece. Fig. 2 shows the welding tools (pin and pinless) that were utilized for the IFSW process. The application of the pin tool in welding the setup (shown in Fig.1c) at one side is referred to as a single-sided IFSW welding while the welding of both Al sides with a pin tool (upper side) and pinless tool (bottom side) is referred to double-sided IFSW welding in this paper. The single and double-sided IFSW processes were performed at varied tool rotational speeds (710, 900, and 1120 rpm) and traverse speeds (21, 40, and 63 mm/min) based on the outcomes of the preliminary study. The preliminary studies were based on the visual assessment of the stirred paths and the hammer impact-knock-off (HIKO) assessment. First, the process parameters of the welds having no surface flow-induced discontinuities or defects were accepted and the resultant/accepted weld samples were subjected to hammer impact-knock off (HIKO) processing. Before the HIKO test, an accepted weld sample was clamped to a bench vice in a manner that the weld line/path was left above the jaws of the vice. Repeated hammer impact loads were progressively employed to bend the weld sample to the righthand side and the reverse/opposite side of the vice respectively until the knockoff of the unclamped section of the weld sample ensued. The weld samples that could not bear up to 3 side-bends were rejected. Based on this, the process parameters were selected for this study. The plates in the single-sided welds were first welded together using a pin tool as shown in Fig.3a and 3b. The double-sided IFSW welding was carried out in a step-wise manner under the same welding conditions except that the pin tool was replaced with the pinless tool for the welding of the bottom side of the Al plates. It should be noted that the plate was turned over in such a way that the advancing side (AS) during the single-sided IFSW welding became the retreating side (RS) during the pinless welding of the opposite/bottom side.

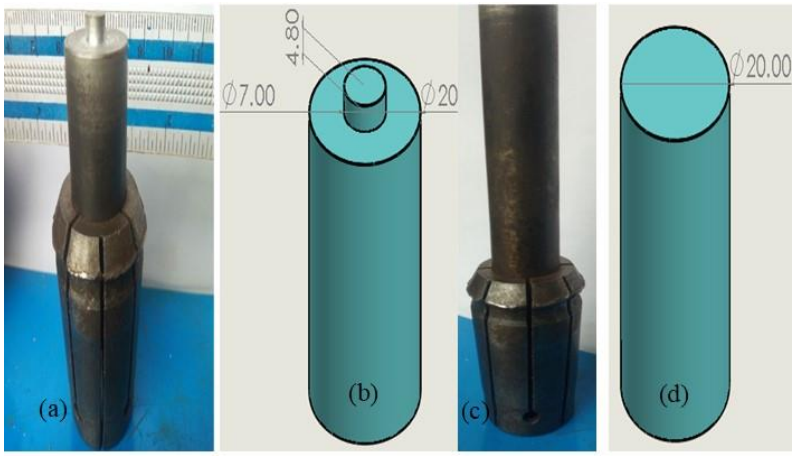

Fig. 2 Welding tool used for the IFSW process: (a) Pin tool with collet, (b) Schematic of the pin tool (c) Pinless tool with collect, (d) Schematic of the pinless tool (All dimensions are in mm)

The single- and double-sided IFSW'ed samples were cut perpendicular to the welding direction, ground, polished, and etched in Keller's reagent (1 ml HF + 1.5 ml HCL + 2.5 mlNHO3 + 95 ml H2O). The microstructure of the etched samples was examined under an OMAX computerized optical microscope (OM). The tensile samples were obtained

according to the illustration shown in Fig.4a. The samples for the tensile test were cut in triplicates perpendicular to the welding direction (see Fig.4b) and subsequently wet milled to the dimensions provided in Fig.4a. For the preparation of the tensile samples, the start and stop (keyhole) ends of the weld sample were cut off via the use of a guillotine machine, and additional 3 cut samples were obtained for the wet milling process. The obtained 3 cut samples were stacked together with two (2) unwelded Al plates. The unwelded plates were placed above and below the weld samples and rigidly clamped before the start of the machining process. The stacked samples were gradually milled to the dimensions provided in Fig.4a under the continuous flow of the soluble oil cutting fluid. The removal of the heat generated (by friction and metal shearing) during the cutting process was aided by the cutting fluid to mitigate the impact of the cutting zone temperature on the samples. The INSTRON 5582 model Universal Testing Machine (UTM) was used to determine the tensile properties of the joint at a strain rate of 5 mm/s according to the ASTM E8M/B557 standard. Scanning Electron Microscope (SEM) was then used to examine the fracture surfaces of the joints.

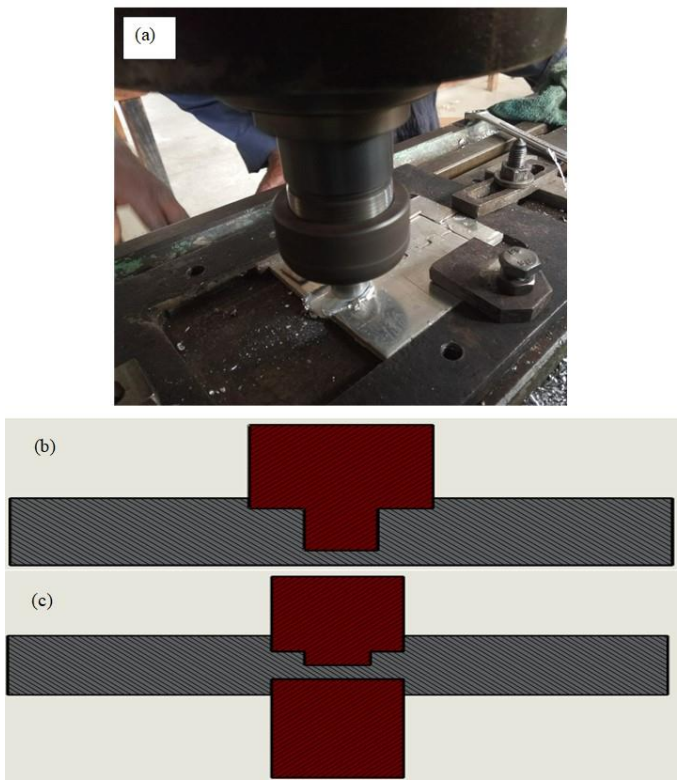

Fig. 3 Schematic representation of the IFSW processes: (a) single-sided IFSW welding (welding of the first side), (b) schematic illustration of the single-sided IFSW, (c) double-sided IFSW welding

3. Results and Discussion

3.1 Surface Appearance and Structure of Welds

The front and back views of the single- and double-sided IFSW welds are shown in Fig.5. The front views of the single and double-sided welds appear to be the same in Fig.5a and

5c due to the processing of the welds with the same pin tool. Deformation/plasticization and tool travel-induced onion rings, exit pinholes, and shearing-induced weld flashes are present on the top surface of the welds in Fig.5a and 5c. The high strain and strain rates attributable to the welding process aid the extrusion of the deformed/plasticized material as the weld flash at the retreating side (RS) of the weld. The interlocking profile remains at the back of the single-sided IFSW weld (see Fig.5b) while the pinless friction stir welding process eliminates this profile in the double-sided IFSW weld (see Fig.5d).

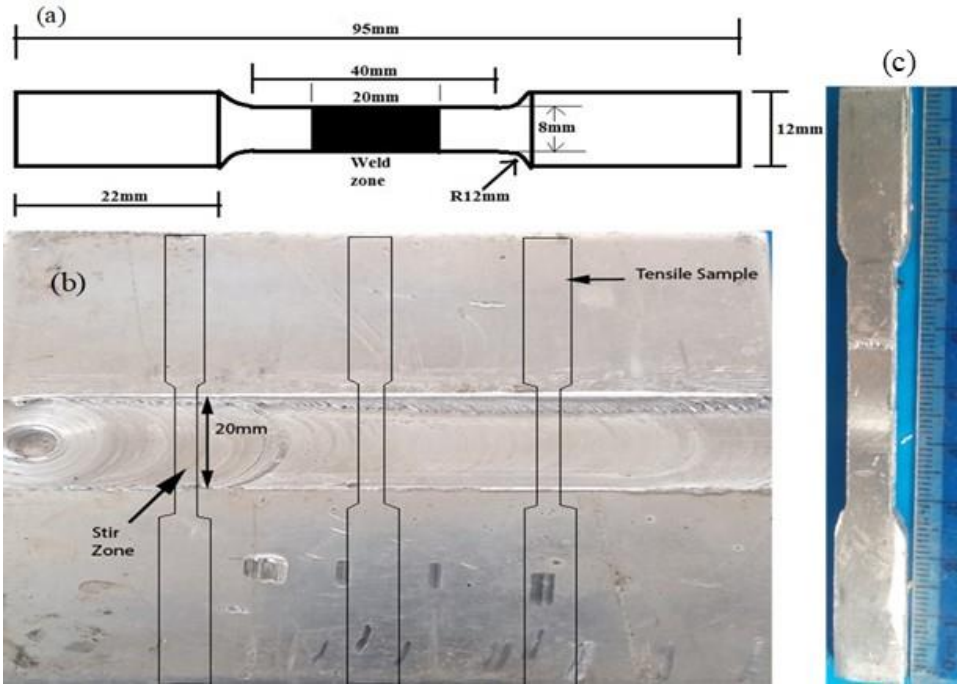

Fig. 4 Tensile test samples: (a) Schematic representation of the tensile sample (b) regions where the tensile samples were taken from on the welded plate (c) sample of the actual tensile sample

traverse speed of 40 mm/min and different rotational speeds (710, 900, and 1120 rpm) are shown in Fig. 6. It is obvious that a change in the tool rotational speed and welding choice (single and double-sided welding) significantly influences the level of flow-induced defects in the IFSW welds (see Fig.6). A similar defect was referred to as a cavity defect in the studies of Du et al. [23] and it was reported that the defect was material flow-related due to the inherent material flow's converging line. The flow-induced defect owing to the new joint configuration shows up as a crack-like defect in the double-sided IFSW weld (see Fig.6d) and as twin crack-like paths along the rise of the joint configuration in the single-sided IFSW welds (see Fig.6a) at 710 rpm. The least area fraction of flow-induced defect is obtained in the IFSW welds produced at 710 rpm in both single and double-sided welds. The increase in the tool rotational speed (from 710 to 900 rpm) caused an increase in the area fraction of the inherent flow-induced defect in the IFSW welds while a decrease in the area fraction of the flow-induced defect ensued as the tool rotational speed was further increased to 1120 rpm (see Fig.6). This behavior could be linked to the non-traditional joint-line morphology (new configuration), variance in heat input, and complex material flow at the interlocked ends of the IFSW welds. To a certain degree, a better inter-material flow (at the joint-lines) and bonding between the interlocked ends of the welds are

obtained in Fig.6a and 6d in relation to the other welds due to satisfactory plasticization at low heat input (at 710 rpm). A further increase in the heat input (at 900 rpm) caused an unsatisfactory flow and a wider flow-defect or flow-induced unbonded span and partly bonded rise (in the single-sided weld in Fig.6b) while tunnel-like flow defects at the corners of the rise were found in the double-sided weld in Fig.6c. The highest heat input (at 1120 rpm) further reduced the inherent flow-induced defect at the joint-line/interlocked end of the joint relative to the samples welded at 900 rpm. It can be affirmed that the increase in the tool rotational speed (from 710 to 1120 rpm) does not have a direct relationship with the area fraction of the inherent flow-induced defect in the IFSW welds owing to the joint configuration.

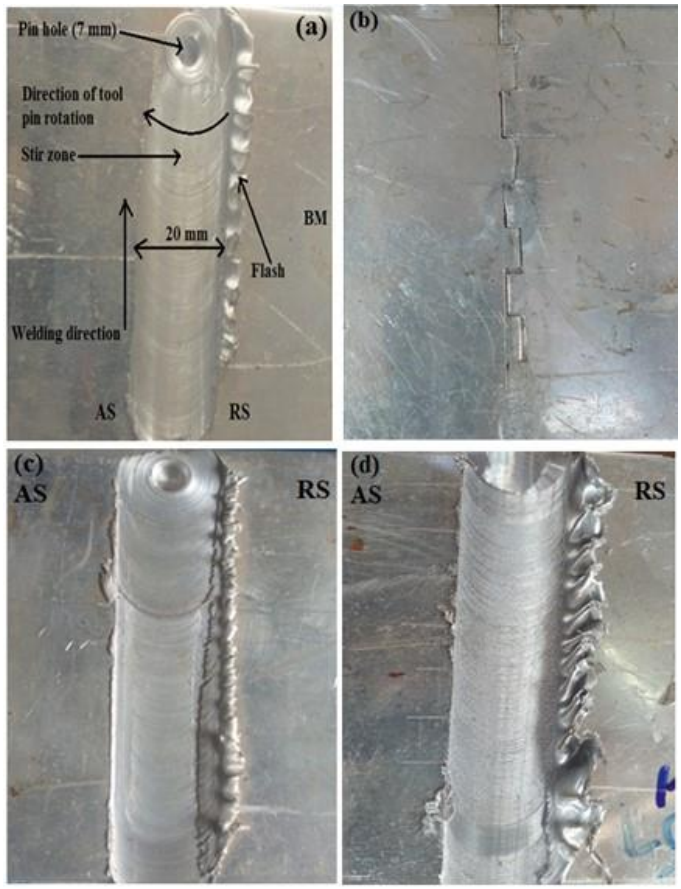

Fig. 5 Surface appearances of IFSW welds: (a) front view of the single-sided IFSW weld (b) Back view of the single-side weld (c) front view of the double-sided IFSW weld (d) Back view of double-sided IFSW weld.

The macrographs of the interlocked friction stir welded (IFSW) joints made at a constant. Meanwhile, some degree of flow defect is found along the interlocked-ends/joint-lines of all the IFSW weld samples (both single and double-sided welds) but the severity of the defect is to some extent reduced in the double-sided welds as compared to the single-sided weld counterparts fabricated under the same process parameters. The double-sided IFSW process is considered to have provided a synergetic combination of pin and pinless-assisted (dual) material plasticization, consolidation of material flow, and twofold

recrystallization effects on the IFSW joint. These phenomena are reckoned to have favored the reduction in the area fraction (level) of the flow-induced defect in the double-sided IFSW welds as compared to their single-sided counterparts in Fig. 6.

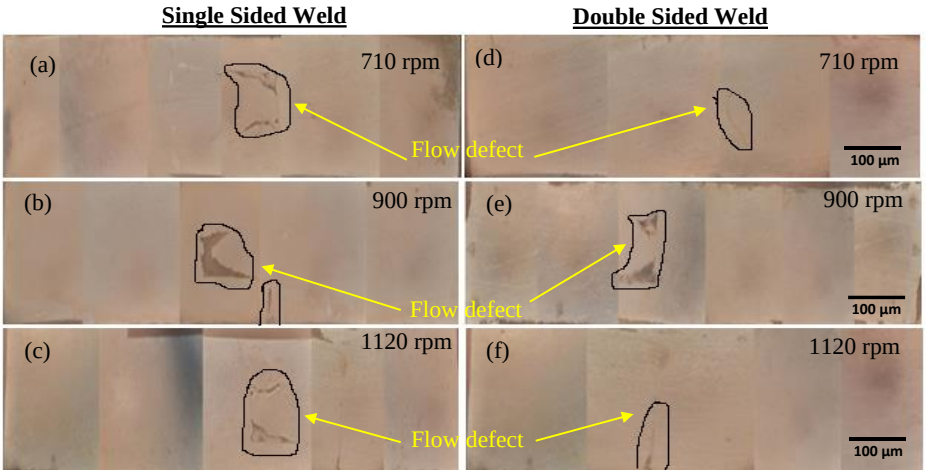

Fig. 6 Macrographs of IFSW welds obtained at constant 40 mm/min and different rotational speeds: single-sided welds at (a) 710 rpm, (b) 900 rpm, (c) 1120 rpm, and double-sided welds at (d) 710 rpm, (e) 900 rpm, and (f) 1120 rpm

Overcoming flow-defect is important for the integrity of the IFSW welds. There are many strategies for lessening or eliminating flow defects such as flash, void, and tunnels in literature [24]. Optimization studies and parameter settings that eliminate abnormal stirring, and excessive or insufficient heat input are required for the prevention of defects in FSW welds [25] [26]. As a result, the flow defect found in this study could be further mitigated via process parameter optimization with appropriate tool designs. It has been reported that optimized heat input and flow behavior, effective selection of FSW parameters, and relatively large tool shoulder with sufficient pin length are necessary for the mitigation of flow defects in FSW Welds [27]. Flow enhancing features such as threading was also acknowledged to aid the elimination of void defect in the studies of Mohammadi-pour et al. [28].

3.2 Tensile Strength of IFSW Welds

Fig. 7 shows the average tensile strengths of the single and double-sided IFSW joints obtained at different processing parameters. The stress-strain curves obtained from the tensile tests are presented in the appendix (Fig. A1 and A2). It is obvious from the plot that the double-sided welds have better tensile strengths compared to that of the single-sided counterparts. The maximum tensile strengths of the single and double-sided IFSW welds are 39.6 and 69.1 MPa respectively (at 700 rpm and 40 mm/min). This is due to the lesser area fraction of flow-induced defect together with the additional pinless tool-induced material consolidation and twofold recrystallization effects in the double-sided IFSW welds. This phenomenon favors a better loadbearing resistance of the double-sided IFSW welds compared to the single-sided IFSW welds having profound and larger area fractions of flow-induced defects along the joint-line/interlocked ends of the IFSW welds. Also, the strengthened welding interface has been reported as a factor responsible for strength improvement in the double-sided friction stir spot welded joints in the studies of Wang et al. [29].

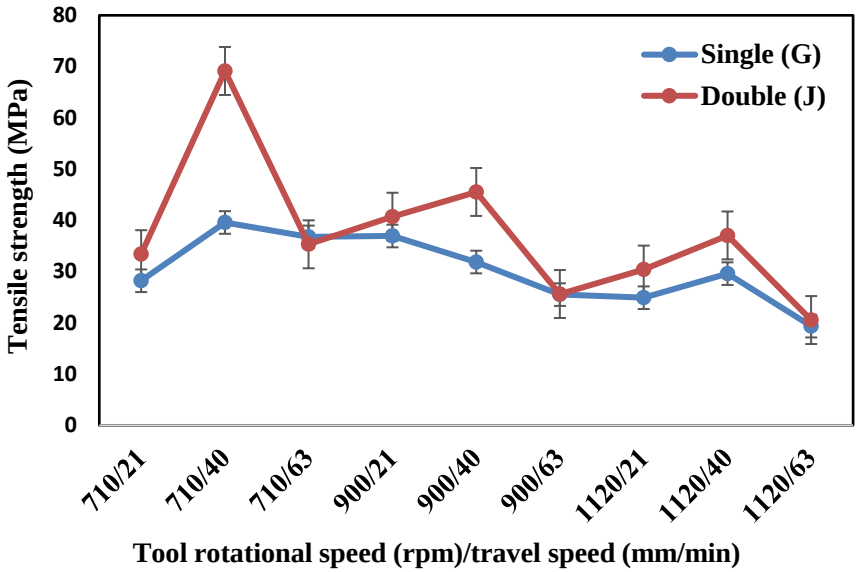

Fig. 7 Effect of varying welding parameters of the tensile strength of single and double-sided IFSW welds of Al-alloy

The assessment of the plot (see Fig.7) reveals that the welds fabricated at 40 mm/min irrespective of the levels (700, 900, and 1120 rpm) of the tool rotational speed show an improvement in the weld strength. The traverse speed of 40 mm/min produced the maximum tensile strength at different tool rotational speeds (see Fig.7) owing to ideal/sufficient material stirring, and heat input required for good metallurgical bonding in the IFSW joints. The tensile strength of the IFSW welds increases as the traverse speed increases from 21 to 40 mm/min and a further increase in the traverse speed to 63 mm/min causes the strength of the welds to decrease. A decline in the tensile strength of the IFSW joints is obtained at traverse speeds below and beyond 40 mm/min due to the prolonged tool stirring (excessive heat input) and insufficient stirring (low heat input) effects respectively.

The increase in tool rotational speed beyond 710 rpm also caused a decline in the tensile strength of the IFSW welds. This occurrence might be attributed to the direct correlation between heat input and tool rotational speed. Elevated temperature or heat input at higher tool rotational speed has been reported to aid thermal softening, and grain coarsening effects in Al alloys [30][31]. This attribute is adjudged to have impaired the tensile strength of the IFSW welds as the tool rotational speed of the weld was increased. Also, the area fraction of the flow-induced defect has been revealed to increase as the tool rotational speed was increased to 900 rpm. These stress-raisers (flow defects) are crack initiation sites in welds and the coalescence of the inherent defects in the samples having profound flow-induced defects leads to quicker weld failure and reduced tensile strength.

3.3 Weld Fracture Behavior

The fracture paths and their equivalent illustrations for the single and double-sided IFSW welds are studied in Fig.8 to understand the fracture behavior of the IFSW welds. The role of the advancing side (AS) and the retreating side (RS) on the weld failure/fracture of the IFSW welds (single and double-sided welds) cannot be ascertained in Fig.8. This might be

due to the dominant influence of the inherent flow defects (at the joint lines) on the failure mode of the IFSW welds.

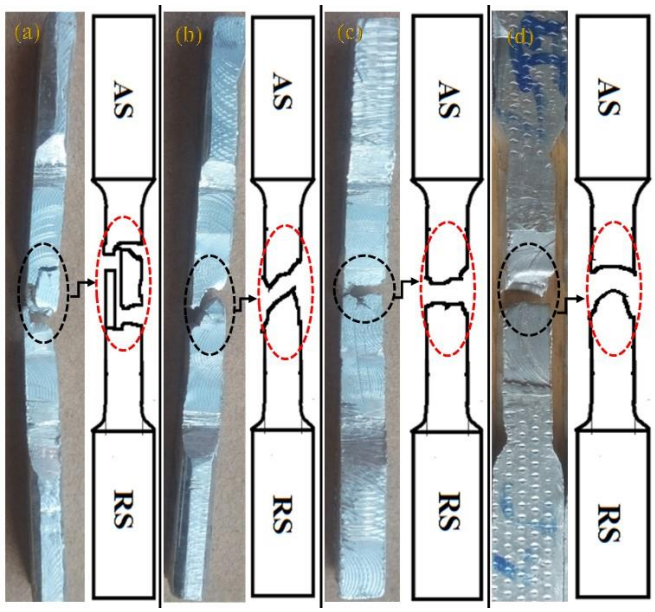

Fig. 8 Fracture paths and their equivalent illustrations for the IFSW welds: (a) single-sided weld at 1120 rpm/40 mm/min, (b) single-sided weld at 710 rpm/40 mm/min, (c) double-sided weld at 1120 rpm/40 mm/min, (d) double-sided weld at 710 rpm/40 mm/min

The fracture path of the single and double-sided IFSW welds takes place along the stirred zone of the joints in Fig.8. However, it is important to note as observed in Fig.8a that the fracture path of the single-sided joint (1120 rpm/40 mm/min) occurred along the joint-line or interlocked ends of the IFSW weld. This is a confirmation of the presence of stress-concentration along the interlocked ends of the weld, and this also provides evidence that the weld offers little loadbearing resistance before its eventual failure upon tensile loading/test. Tang et al. [32] reported that the micro-void features (of the zigzag line defect) in the FSW weld promoted crack propagation under loading. Meanwhile, the single-sided IFSW weld fabricated at 710 rpm/40 mm/min (see Fig.8b) shows a fracture path across the bonded joint-line of the weld, which is contrary to that of Fig.8a. The deviation of the fracture path away from the interlocked ends/paths (see Fig.8b) confirms that the tensile strength of the single-sided weld (obtained at 710 rpm/40 mm/min) to be better than that of Fig.8a. On the other hand, the fracture paths of the double-sided IFSW welds (see Fig.8c and d) are close to that of the single-sided one in Fig.8b, which also confirms that the weld failure is not significantly influenced by the bonded joint-line (interlocked ends). The inherent flow defect in the double-sided IFSW weld produced at 1120 rpm/40 mm/min (see Fig.8c) aids the failure across the joint whereas some level of ductility is experienced by its counterpart welded at 710 rpm/40 mm/min.

Fig. 9 shows and compares the fracture surfaces of the failed IFSW samples after the tensile tests. Flow-induced macro/micro-defects and mixed fracture (brittle and ductile) characterized the fracture surfaces of the single-sided welds in Fig.9a-c whereas the surfaces of the double-sided welds were predominated by ductile fractures in Fig.9d-f. The single-sided weld fabricated at 710 rpm and 40 mm/min had a flow defect (tunnel-like)

surrounded by uneven fracture layers having large dimples and brittle-like appearances in Fig.9a. Apart from the stress raiser (flow defect) in Fig.9a, the fracture features of the weld confirm that mixed fracture (with a large area fraction of ductile mode) ensued in the single-sided IFSW weld. This occurrence justifies the improved tensile strength of the single-sided joint fabricated at 710 rpm and 40 mm/min as compared to the other single-sided welds having brittle/mixed fracture appearances in Fig.9b and c. Flow-induced cavities with minimal ductile features are present in the single-sided weld produced at 900 rpm and 40 mm/min (see Fig.9b) while the presence of brittle facets and a few dimple appearances are found in the single-sided weld produced at 1120 rpm and 40 mm/min (see Fig.9c). It can be concluded that mixed fracture mode occurs in Fig.9b and c. On the other hand, the double-sided welding process significantly improved the IFSW welds (see Fig.9d-f) by significantly reducing the flow defects and making the welds exhibit some level of ductility and loadbearing attributes. For instance, the double-sided welds produced at 710 rpm and 40 mm/min (see Fig.9d) and at 900 rpm and 40 mm/min (see Fig.9e) have predominantly shallow and some large dimples. This observation is a confirmation of ductile fracture modes in the welds. This is in agreement with the studies of Xu et al [33] as large dimples on the fracture sites were reported as evidence of ductile fracture mode. Fig.9f also confirms the presence of some fine dimples and a flow defect (see the enclosed orange circle in Fig.9f) in the double-sided weld produced at 1120 rpm and 40 mm/min. This occurrence validates that the double-sided welding process improves the weld strength of the IFSW joints via attributes such as reduction in flow-induced defects, improved plasticization/material flow, and twofold recrystallization phenomena.

4. Conclusion

Weldability of the interlock-end friction stir welding (IFSW) of the AA1050 aluminum alloy was successfully investigated by employing single- and double-sided welding procedures. The structure, tensile strength, and fracture patterns of the single- and double-sided IFSW welds fabricated at different process parameters were studied and compared. The following findings were observed from this investigation:

- The joint lines of the interlocked friction stir welded (IFSW) joint have flow-induced defects in both weld categories (single- and double-sided IFSW welds) owing to the interlocked morphology.
- The severity of the inherent flow defect in the IFSW welds is significantly reduced in the double-sided IFSW welds as compared to the single-sided counterparts due to the advantage of dual material plasticization, material consolidation, and twofold recrystallization effects in the double-sided IFSW welds.
- The increase in the tool rotational speed (from 710 -1120 rpm) does not have a direct correlation with the area fraction of the inherent flow-induced defect in the IFSW joint.
- The double-sided welds have better tensile strengths compared to the single-sided weld counterparts due to the lesser area fraction of flow-induced defect or stress raiser. The maximum tensile strengths of the single and double-sided IFSW welds were 39.6 and 69.1 MPa respectively.
- The tensile strength of the IFSW welds increases as the traverse speed increases from 21 to 40 mm/min and a further increase in the traverse speed to 63 mm/min causes the strength of the welds to decrease.
- The fracture path/location of the single and double-sided IFSW welds takes place along the stir zone. The rotating tool-aided advancing and retreating sides do not influence the weld fracture location of the IFSW welds owing to the dominant influence of flow defect on the weld failure.

- A large expanse of ductile fracture features and brittle appearances characterized the fracture surfaces of the single and double-sided IFSW welds respectively.

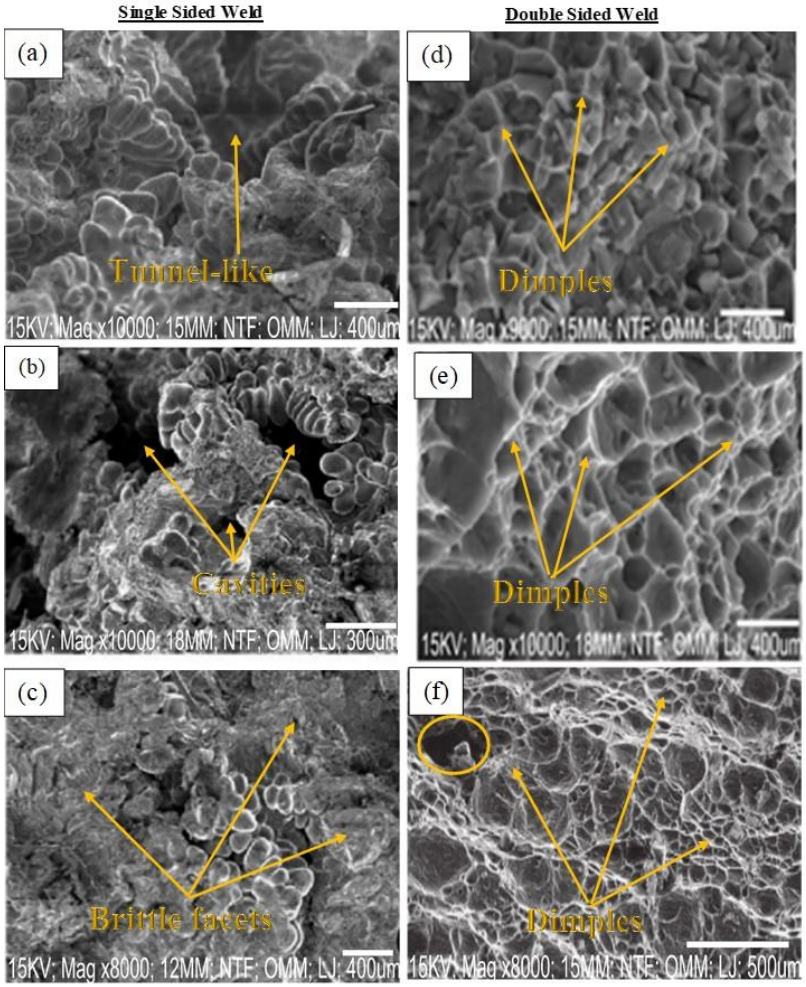

Fig. 12. Fracture surfaces of the IFSW welds: the single-sided welds at (a) 710 rpm/40 mm/min, (b) 900 rpm/40 mm/min, (c) 1120 rpm/40 mm/min; and double-sided welds at (d) 710 rpm/40 mm/min, (e) 900 rpm/40 mm/min, (f) 1120 rpm/40 mm/min

References

[1] Thakur R, Bajwa PS. Friction stir welding of 5xxx series aluminum alloys: A literature survey. International Journal of Scientific Research in Science, Engineering, and Technology, 2016; 2(2): 1129-1131.

[2] Qiao Q, Su Y, Li Z, Cui Q, Yu H, Ouyang Q, Zhang D. Effect of overlapping region on double-sided friction stir welded joint of 120 mm ultra-thick SiCp/Al composite plates. Materials Science & Engineering A, 2020; 782: 139238. https://doi.org/10.1016/j.msea.2020.139238

[3] Hejazi I, Mirsalehi SE. Effect of pin penetration depth on double-sided friction stir welded joints of AA6061-T913 alloy. Transaction of Nonferrous Metals Society of China, 2016; 26: 676 - 683. https://doi.org/10.1016/s1003-6326(16)64158-4

[4] Ma ZY, Feng AH, Chen DL, Shen J. Recent Advances in Friction Stir Welding/Processing of Aluminium Alloys: Microstructural Evolution and Mechanical Properties. Critical Reviews in Solid State and Materials Sciences, 2018; 43(4): 269-333. https://doi.org/10.1080/10408436.2017.1358145
[5] Pankul G, Arshad NS, Noor ZK, Mohd AH, Zahid AK, Mustufa HA, Abdulrahman A. Investigation on the Effect of Tool Pin Profiles on Mechanical and Microstructural Properties of Friction Stir Butt and Scarf Welded Aluminium Alloy 6063. Metals, 2018; 8(1): 74. https://doi.org/10.3390/met8010074
[6] Darmadi DB, Talice M. Improving the strength of friction stir welded joint by double side friction welding and varying pin geometry. Engineering Science and Technology, an International Journal, 2020; 24(3): 637-647. https://doi.org/10.1016/j.jestch.2020.11.001
[7] Ojo OO, Taban E, Kaluc E. Understanding the role of welding parameters and tool profile on the morphology and properties of expelled flash of spot welds. Materials and Design, 2016; 108: 518-528. https://doi.org/10.1016/j.matdes.2016.07.013
[8] Xu W, Wang H, Luo Y, Li W, Fu MW. Mechanical behavior of 7085-T7452 aluminum alloy thick plate joint produced by double-sided friction stir welding: Effect of welding parameters and strain rates. Journal of Manufacturing Processes, 2018; 35: 261-270. https://doi.org/10.1016/j.jmapro.2018.07.028
[9] Zhou M, Morisada Y, Fujii H; Ishikawa, T. Mechanical properties optimization of AZX612-Mg alloy joint by double-sided friction stir welding. Journal of Materials Processing Tech., 2018; 254: 91-99. https://doi.org/10.1016/j.jmatprotec.2017.11.014
[10] Chen J, Fujii H, Yufeng SY, Morisada Y, Kondoh K. Optimization of mechanical properties of fine-grained non-combustive magnesium alloy joint by asymmetrical double-sided friction stir welding. Journal of Materials Processing Technology, 2017; 242: 117-125. http://dx.doi.org/10.1016/j.jmatprotec.2016.11.021
[11] Kumar U, Acharya U, Saha SC, Roy BS. Microstructure and mechanical property of friction stir welded Al-Mg joints by adopting modified joint configuration technique. Materials Today: Proceedings, 2020; 26: 2083-2088. https://doi.org/10.1016/j.matpr.2020.02.450
[12] Paidar M, Ojo OO, Ezatpour HR, Heidarzadeh A. Influence of multi-pass FSP on the microstructure, mechanical properties and tribological characterization of Al/B4C composite fabricated by accumulative roll bonding (ARB). Surface and Coatings Technology, 2019; 361: 159-169. https://doi.org/10.1016/j.surfcoat.2019.01.043
[13] Chu Q, Li WY, Hou HL, Yang XW, Vairis A, Wang C, Wang WB. On the double-side probeless friction stir spot welding of AA2198 Al-Li alloy. Journal of Materials Science & Technology, 2019; 35: 784–789. https://doi.org/10.1016/j.jmst.2018.10.027
[14] Yang C, Zhang JF, Ma GN, Wu LH, Zhang XM, He GZ, Xue P, Ni DR, Xiao BL, Wang KS, Ma ZY. Microstructure and mechanical properties of double-side friction stir welded 6082Al ultra-thick plates. Journal of Materials Science & Technology, 2020; 41: 105-116. https://doi.org/10.1016/j.jmst.2019.10.005
[15] Bhardwaj N, Narayanan RG, Dixit US, Hashmi MSJ. Recent developments in friction stir welding and resulting industrial practices. Advances in Materials and Processing Technologies, 2019; (5)3: 461-496. https://doi.org/10.1080/2374068x.2019.1631065
[16] Reza-E-Rabby MD, Ross K, Whalen S, Hovanski Y, McDonnell M. Solid-State Joining of Thick-Section Dissimilar Materials Using a New Friction Stir Dovetailing (FSD) Process. The Minerals, Metals and Materials Series, 2017; 67-77. https://doi.org/10.1007/978-3-319-52383-5_8
[17] Yan Z, Liu X, Fang H. Effect of sheet configuration on microstructure and Mechanical Behaviors of Dissimilar Al-Mg-Si/Al-Zn-Mg Aluminium Alloys Friction Stir Welding

Joints. Journal of Materials Science and Technology, 2016; 32(12): 1378 – 1385. https://doi.org/10.1016/j.jmst.2016.10.011
[18] Li Z, Zhang Y, Shen W, Hu LL. Dissimilar friction stir welding of Ti–6Al–4V alloy and aluminum alloy employing a modified butt joint configuration: Influences of process variables on the weld interfaces and tensile properties, Materials & Design 2014; 53: 838-848. https://doi.org/10.1016/j.matdes.2013.07.019
[19] Acharya U, Medhi T, Sethi D, Choudhury S, Banik A, Saha SC, Roy BS. A study on the implication of modified joint configuration in Friction stir welding. Soldagem & Inspeção, 2021; 26: 2606. https://doi.org/10.1590/0104-9224/SI26.07
[20] Sethi D, Acharya U, Shekhar S, Roy BS. Applicability of unique scarf joint configuration in friction stir welding of AA6061-T6: Analysis of torque, force, microstructure, and mechanical properties, Defence Technology. 2021; 1-16. https://doi.org/10.1016/j.dt.2021.03.010
[21] Zhang W, Shen Y, Yan Y, Guo R. Dissimilar friction stir welding of 6061 Al to T2 pure Cu adopting tooth shaped joint configuration: Microstructure and mechanical properties. Materials Science & Engineering A, 2017; 690: 355 – 364. http://dx.doi.org/10.1016/j.msea.2017.02.091355–364
[22] Mhedhbi M, Khlif M, Bradai C. Investigations of microstructural and mechanical properties evolution of AA1050 alloy sheets deformed by cold-rolling process and heat treatment annealing. Journal of Materials and Environmental Sciences, 2017; 8: 2967-2974
[23] Du S, Liu H, Jian M, Hu Y, Zhou L. Eliminating the cavity defect and improving mechanical properties of TA5 alloy joint by titanium alloy supporting friction stir welding. Journal of Manufacturing Processes, 2021; 69: 215-222. https://doi.org/10.1016/j.jmapro.2021.07.044
[24] Ojo OO, Taban E. Hybrid multi-response optimization of friction stir spot welds: failure load, effective bonded size and flash volume as responses. Sadhana, 2018; 43(6): 1-13. https://doi.org/10.1007/s12046-018-0882-2
[25] Suresh S, Elango N, Venkatesan K, Lim WH, Palanikumar K, Rajesh S. Sustainable friction stir spot welding of 6061-T6 aluminum alloy using improved non-dominated sorting teaching learning algorithm. Journal of Materials Research Technology, 2020; 9: 11650-11674. https://doi.org/10.1016/j.jmrt.2020.08.043
[26] Dialami N, Cervera M, Chiumenti M. Defect formation and material flow in Friction Stir Welding. European Journal of Mechanics / A Solids, 2020; 80: 103912. https://doi.org/10.1016/j.euromechsol.2019.103912
[27] Kah P, Rajan R, Martikainen J, Suoranta R. Investigation of weld defects in friction-stir welding and fusion welding of aluminum alloys. International Journal of Mechanical and Materials Engineering, 2015; 10:26. https://doi.org/10.1186/s40712-015-0053-8
[28] Mohammadi-pour M, Khodabandeh A, Mohammadi-pour S, Paidar M. Microstructure and mechanical properties of joints welded by friction-stir welding in aluminum alloy 7075-T6 plates for aerospace application. Rare Metals, 2016. https://doi.org/10.1007/s12598-016-0692-9
[29] Wang X, Morisada Y, Ushioda K, Fujii H. Double-sided friction stir spot welding of ultra-high-strength C-Mn-Si martensitic steel by adjustable probes. Journal of Materials Processing Technology, 2022; 300: 117422. https://doi.org/10.1016/j.jmatprotec.2021.117422
[30] Ojo OO, Taban E, Kaluc, E. Friction stir spot welding of aluminum alloys: a review. Materials Testing, 2015; 57(7-8): 609-627. https://doi.org/10.3139/120.110752
[31] Heydari F, Amadeh A, Ojo OO, Hasanniya MH, Tamizifar M. Microstructure and mechanical properties of autobody steel joined by friction stir spot welding, Sādhanā 2019; 44(3): 1-10. https://doi.org/10.1007/s12046-019-1057-5

[32] Tang W, Yang X, Li S, Li H. Zigzag line defect in friction stir butt-weld of ferritic stainless steel. Materials Letter, 2021; 288: 129361. https://doi.org/10.1016/j.matlet.2021.129361

[33] Xu X, Liu Q, Hou H, Wang J, Ren X. Effect of incomplete penetration defects on mechanical and fatigue properties of friction-stir-welded 6802-T6 joint. Journal of Materials Research and Technology, 2021; 15: 4021-4031. https://doi.org/10.1016/j.jmrt.2021.10.028

Appendix

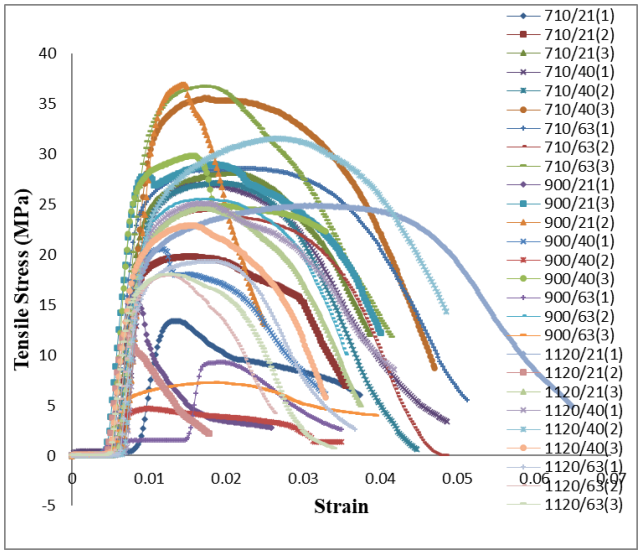

Fig. A1. Stress-strain curves of the single-sided IFSW welds

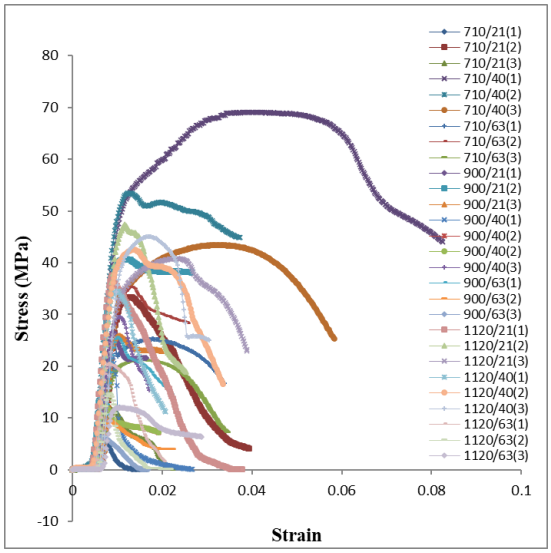

Fig. A2. Stress-strain curves of the double-sided IFSW welds